Asia-Pac. J. Atmos. Sci., 53(1), 85-100, 2017
DOI:10.1007/s13143-017-0007-6
pISSN 1976-7633 / eISSN 1976-7951

Amplitude-Dependent Relationship Between the Southern Annular Mode and the El Niño Southern Oscillation in Austral Summer

Baek-Min Kim[1], Hyesun Choi[1,2], Seong-Joong Kim[1], and Wookap Choi[2]

[1]*Korea Polar Research Institute, Incheon, Korea*
[2]*School of Earth and Environmental Sciences, Seoul National University, Seoul, Korea*

(Manuscript received 22 June 2016; accepted 30 September 2016)

Abstract: Co-variability between the Southern Annular Mode (SAM) and the El Niño Southern Oscillation (ENSO) during the austral summer is examined, and it is found that there exists an apparent co-variability of a negative (positive) SAM during the mature period of El Niño (La Niña). However, this co-variability is largely controlled by the small number of strong ENSO cases. When strong ENSO cases are excluded, the correlation becomes non-significant. This behavior in the relationship between SAM and ENSO is supported by a series of general circulation model experiments with prescribed sea surface temperature boundary conditions that represent the incremental strengthening of El Niño (La Niña) conditions. The modeled Antarctic sub-polar jet exhibits similar behavior to that identified through observational analysis. Marked changes in both the magnitude and position of the sub-polar jet are largely controlled by particularly strong transient eddy forcing. Planetary wave forcing plays only a minor role in the co-variability, but it can explain in part the asymmetric response of the sub-polar jet between El Niño and La Niña.

Key words: Southern Hemisphere sub-polar jet (SPJ), Southern Annular Mode (SAM), El Niño Southern Oscillation (ENSO), transient eddy forcing

1. Introduction

The El Niño Southern Oscillation (ENSO) is a leading climate mode in the tropics that has significant impacts on ecosystems and global climate (e.g., Hoerling and Ting, 1994; Trenberth and Hurrell, 1994; Straus and Shukla, 1997; Compo and Sardeshmukh, 2004; Schubert et al., 2004a, 2004b; Orlanski, 2005; Seager et al., 2005, 2008; Eichler and Higgins, 2006; Seager, 2007). A number of previous studies have investigated the influence of ENSO on the Antarctic climate in austral summer through modulation of the Southern Annular Mode (SAM) or other circulation links (e.g., Harangozo, 2000; Robinson, 2000; Kwok and Comiso, 2002; Turner et al., 2009; Ding et al., 2011, 2012; Gong et al., 2013; Lim et al., 2013; Wang and Cai, 2013).

In the extratropical Southern Hemisphere, the leading mode of large-scale variability is the SAM, which is characterized by north-south vacillation of the sub-polar jet (SPJ), and exhibits a dipole pattern in the westerly wind anomaly with centers near 40°S and 65°S (e.g., Kidson, 1988; Gong and Wang, 1998; Thompson and Wallace, 2000). Although the SAM is considered a self-oscillatory internal mode of variability with a time-scale of a few weeks, its phase is largely modulated by the influence of variability in the tropical sea surface temperature (SST). The modulating effect of tropical SST is especially significant during the austral summer season when the climatological position of the SPJ is closer to the subtropical jet such that the tropical influence can more easily affect the extratropical eddies (e.g., Karoly, 1989; Lu et al., 2008).

ENSO modulation of the zonal-mean eddy-driven jet in the Southern Hemisphere has been investigated in a number of studies, which have evaluated the changes in the subtropical jet as subtropical thermal winds respond to ENSO-induced tropical warming or cooling (e.g., Hoskins and Karoly, 1981; Kushnir et al., 2002; Hartmann, 2007). The resulting enhanced/suppressed vertical wind shear is accompanied by low-level baroclinicity in the extratropics, which enhances/suppresses the upward eddy activity flux of baroclinic waves (e.g., Robinson, 2002). Consequently, the eddy-driven jet shifts along with the changes in the extratropical wave activity flux (e.g., Lorenz and Hartmann, 2001; Chen and Plumb, 2009; Zurita-Gotor et al., 2014). Changes in the subtropical westerly winds during ENSO also alter the critical latitude where transient eddies are absorbed. During El Niño, the critical latitude moves equatorward because of the enhanced westerly winds; therefore, the SPJ also moves toward the equator (e.g., Chen and Zurita-Gotor, 2008; Rivière, 2009; Barnes et al., 2010; Harnik et al., 2010; Wang and Magnusdottir, 2011; Lu et al., 2014; Nie et al., 2014). Because the variability in the SAM is essentially an intermittent latitudinal shift of the zonal-mean eddy-driven jet, the above listed mechanisms provide a solid theoretical background for evaluating the relationship between SAM and ENSO in detail.

L'Heureux and Thompson (2006) (hereafter LT) found a linear correlation of −0.52 between the cold tongue index (CTI; a measure of ENSO) and the SAM index during austral summer months (i.e., November to February), which implies that the SAM index for austral summer tends to be positive during La Niña and negative during El Niño. This obser-

Corresponding Author: Seong-Joong Kim, Korea Polar Research Institute, PO Box 32, Incheon 21990, Korea.
E-mail: seongjkim@kopri.re.kr

vational finding seems to be consistent with the aforementioned modeling studies and theoretical arguments. Gong et al. (2010) revisited the findings of LT by showing that the frequency of intra-seasonal SAM events is strongly skewed toward one particular phase during ENSO events. They suggested that the tropospheric background flow associated with La Niña (El Niño) favors strong (weak) wave breaking, and the associated eddy forcing tends to drive the SAM into a positive (negative) phase. However, this relationship is not robust through time. Wang and Cai (2013) argued that the SAM and ENSO relationship exhibits multi-decadal fluctuations, and sometimes they show the opposite relationship.

Through observational analysis and a series of modeling experiments, this study investigates following questions: (1) What are the relative contribution of stationary and transient eddy forcings during ENSO to the maintenance of the southern SPJ during austral summer? (2) Do these forcings increase linearly with respect to the strength of tropical ENSO forcing, and if so, how strong is the link, and what is the physical mechanism of enhanced or reduced eddy forcing during ENSO? (3) Do ENSO-driven extratropical SST anomalies play a role in this SAM-ENSO linkage? To address these issues, we investigate the sensitivity of the SAM to the unusual increases of SST forcing associated with both El Niño and La Niña separately. The contribution of eddy forcing induced by ENSO is quantitatively assessed.

The paper is organized as follows. Data, analytical methods, and a brief description on the model used for this study are discussed in section 2. Observational evidence of the amplitude-dependent relationship between the SAM and ENSO is presented in section 3a. The responses of mean flow and eddy forcing in both observational and model analysis with different ENSO amplitudes are shown in section 3b. The discussion and final remarks are presented in section 4.

2. Data and methods

For the present study, the SAM index is defined as the difference in normalized monthly zonal-mean sea-level pressure between 40°S and 65°S (e.g., Marshall, 2003). We obtained the observation-based SAM index data from an online database (http://www.antarctica.ac.uk/met/gjma/sam.html). To represent ENSO, we adopted the conventional Niño 3.4 index following the definition of the Climate Prediction Center (CPC) (http://www.cpc.ncep.noaa.gov/data/indices/). The ENSO index data [i.e., the Oceanic Niño Index (ONI) or simply the Niño 3.4 index] were obtained from a 3-month running mean of the Extended Reconstructed SST version 3b (ERSST.v3b SST) anomalies dataset in the Niño 3.4 region based on base periods updated every 5 years (Smith et al., 2008). LT examined the SAM-ENSO relationship using different ENSO indices such as CTI, which uses SST anomalies averaged over a domain slightly different from Niño 3.4 to emphasize more strongly the SST variability in the eastern Pacific. The CTI used in this study is available online from the Joint Institute for the Study of the Atmosphere and Ocean (JISAO) at the University of Washington (http://www.jisao.washington.edu/data/cti/). We found a strong correlation between the CTI and ONI, which indicates that these two datasets represent virtually identical ENSO phenomena. For the correlation analysis, we used two different ENSO indices (Niño 3.4 and CTI) to assess the sensitivity of the correlation for each index (Table 2).

To investigate the relationship between SAM and ENSO in detail, we classified each year from 1957 to 2013 into five categories (Table 1). The El Niño and La Niña episodes are defined as the times when a threshold of anomalies of +/–0.5°C SST are met for a minimum five consecutive, overlapping seasons. Categorization of El Niño and La Niña episodes as strong or moderate is based on the DJF (December-

Table 2. Correlations of the ENSO index with the SAM index calculated using whole years from 1957 to 2013 for Niño 3.4, 1957 to 2010 for CTI (second row), and years of the different ENSO strengths in Table 1 (third and fourth row). DJF averaged values are used for the correlation analysis. Bold type and asterisks indicate significance levels of 95% and 99%, respectively, estimated using a two-tailed Student's *t*-test. The values in parentheses refer to sampling numbers.

	Case	Niño 3.4 (1957-2013)	CTI (1957-2010)
1	Total	**–0.29 (57)**	**–0.27 (54)**
2	Strong ENSO	**–0.82* (12)**	**–0.82* (12)**
3	Moderate ENSO	+0.18 (25)	+0.20 (22)

Table 1. Five categories of ENSO events based on the magnitude of the Niño 3.4 index averaged over December-February from 1957 to 2013. Note that the years refer to the December. "C" indicates the central Pacific El Niño case, and "E" indicates the eastern Pacific El Niño. Cases are classified according to the definitions of Yu et al. (2015).

Case	Year
Normal (–0.5°C < Niño 3.4 < 0.5°C)	1959, 1960, 1961, 1962, 1966, 1967, 1978, 1979, 1980, 1981, 1985, 1989, 1990, 1992, 1993, 1996, 2001, 2003, 2012, 2013
Strong El Niño (Niño 3.4 ≥ 1.5°C)	1957 (C), 1972 (E), 1982 (E), 1991 (C), 1997 (E), 2009 (C)
Strong La Niña (Niño 3.4 ≤ –1.5°C)	1973, 1975, 1988, 1998, 1999, 2007
Moderate El Niño (0.5°C ≤ Niño 3.4 < 1.5°C)	1958 (C), 1963 (C), 1965 (C), 1968 (C), 1969 (E), 1976 (E), 1977 (C), 1986 (C), 1987 (C), 1994 (C), 2002 (C), 2004 (C), 2006 (E)
Moderate La Niña (–1.5°C < Niño 3.4 ≤ –0.5°C)	1964, 1970, 1971, 1974, 1983, 1984, 1995, 2000, 2005, 2008, 2010, 2011

January-February)-mean Niño 3.4 index because our focus is the austral summer season. Strong ENSO events are defined as years when the DJF Niño 3.4 index exceeds a threshold of +/–1.5°C, whereas moderate events are the years with indices between +/–0.5°C and +/–1.5°C.

In this study, we do not consider the diversity of ENSO types although, in recent decades, different types of ENSOs from the conventional type (i.e., the Central-Pacific ENSO) have been identified in several studies (e.g., Kug et al., 2009). This can be partly justified because Lim et al. (2013) showed that, during austral summer, the SAM-ENSO relationship is largely governed by the traditional cold-tongue type ENSO. Warm-pool type ENSOs play a modulating role for the SAM during the austral cold season, even though their impact is relatively minor. Therefore, to reduce complexity in the interpretation of observational analyses and model simulations, we just use Niño 3.4 index for the ENSO detection. Interestingly, moderate El Niño years are categorized as dominantly central Pacific El Niño. This is contrasting with the strong El Niño cases, which are evenly distributed between the two kinds of El Niño (Table 1). However, investigating how the ENSO-SAM relationship is modulated by different flavors of El Niño is beyond the scope of this study.

The data used in this research are daily mean values of the Japanese 55-year Reanalysis (JRA-55) from the Japan Meteorological Agency (Kobayashi et al., 2015). The horizontal resolution of JRA-55 is TL319, which corresponds to approximately 55 km in a reduced Gaussian grid. We used data for the SH from 1957 to 2013 for 37 vertical levels from 1000 hPa to 1 hPa. The dataset included fields for geopotential height, horizontal wind, and temperature.

As a quantitative measure of eddy forcing, we calculated Eliassen-Palm (EP) flux divergence (Edmon et al., 1980; Andrews et al., 1987) for both the observational and model analyses for both transient and stationary eddies.

The National Center for Atmospheric Research (NCAR) Community Atmospheric Model version 3 (CAM3), which is the atmospheric component model of the NCAR Community Climate System Model version 3 (CCSM3), was used to model the response of the Antarctic SPJ to changes in tropical SST variabilities (i.e., ENSO amplitudes). The general circulation model (GCM) output was given on grids of approximately 2 degrees and 26 vertical sigma levels. The Hadley Centre Sea Ice and Sea Surface Temperature (HadISST) dataset (Rayner et al., 2003) was used to prepare lower boundary conditions for the model simulations. Based on the data presented in Table 1, we prepared composite annual cycles of the SST anomalies for cases of strong El Niño and strong La Niña using the years after 1979. We multiplied both SST anomalies by the amplification factor (α), which may be one of three values from 0.5, 1, or 1.5. Note that $\alpha = 0.5$ and $\alpha = 1$ cases can be compared to the moderate and strong ENSO cases in the observed composite analysis, respectively. Finally, these six SST anomalies with different amplitudes were superimposed onto the composite annual SST cycle for normal years after 1979, as shown in Table 1. A total of seven boundary forcings consist of three El Niño and La Niña forcings with different strengths and one normal year forcing with an amplification factor of 0 (Fig. 2). Each prescribed SST annual cycle is repeated for each modeling experiment for the simulation years; 140 years were modeled. For first 40 years, the model output was discarded, and for the last 100 years, the austral summer seasons (DJF) were analyzed. Because our season of interest is the austral summer (i.e., December-February), composite annual cycles were composed using monthly SST from March of the selected year to February of the following year. Note that global SST distributions for the corresponding ENSO cases were used as boundary conditions in the above experiments.

In this study, the model simulation based on the normal year forcing was considered as the climatological simulation. The observational climatological fields were calculated using averaged values based on the normal years in Table 1. The anomalies were defined as departures from the climatological fields. The significance of the anomalies was tested using two-tailed Student's t test.

3. Results

a. Observational analysis

Figure 1a shows the time series of austral summer (December-February) averaged values of the ENSO and SAM

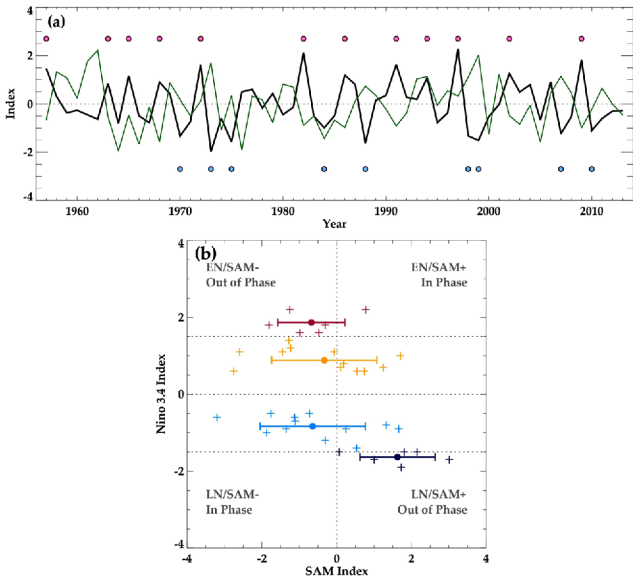

Fig. 1. (a) Time series of SAM (solid green line) and Niño 3.4 (solid black line) indices for 1957-2013. Both indices are DJF averaged values. Red and blue circles indicate the SE and SL years, respectively. (b) Scatter plot of DJF-averaged ENSO-SAM indices for 1957-2013. Crosses with red/orange and navy/sky-blue colors indicate the SE/ME and SL/ML years, respectively. Mean value of SAM indices for each group is represented by closed circle and its error bar (one standard deviation) is indicated. Niño 3.4 index has units of °C.

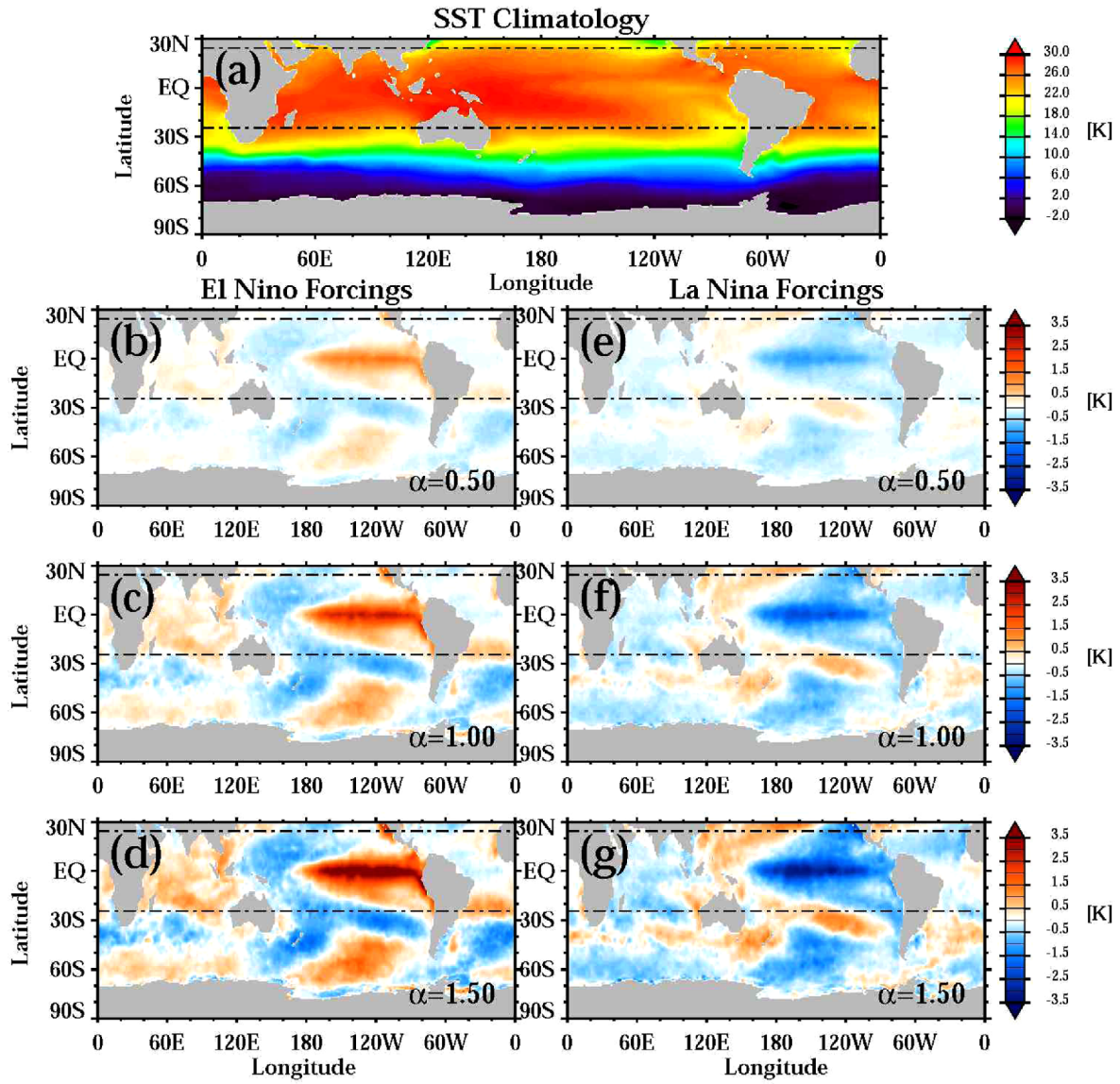

Fig. 2. (a) HadISST January climatology and anomalies for cases of (b-d) El Niño and (e-g) La Niña. From top to bottom, the anomalies are multiplied by amplification factors with (b, e) $\alpha = 0.5$, (c, f) $\alpha = 1.0$, and (d, g) $\alpha = 1.5$. The latitudinal band between two horizontal dashed dotted lines for each panel indicates the forcing region for the T-ENSO experiments.

indices for 1957-2013. Over these 57 years, six strong El Niño events (SE, red circle) and six strong La Niña events (SL, blue circle) were identified according to the ENSO criteria summarized in Table 1. For these strong cases, an out-of-phase relationship between the SAM and ENSO indices is obvious.

The relationship between ENSO and the SAM indices is more apparently recognized in the scatter diagram (Fig. 1b). Among the six SE years, the SAM phases were negative for five of the years, whereas the SAM phases for the six SL years were consistently positive. This result reconfirms the reported negative relationship between ENSO and the SAM that appears to be dominant during strong ENSO periods. However, in cases of moderate ENSO, this relationship disappears (Table 1 lists specific years of moderate ENSO events); i.e. the SAM indices are evenly distributed among both El Niño and La Niña phases. Non-ENSO years are excluded. Because the majority of ENSO events are moderate cases, the results of LT and Gong et al. (2010) must be interpreted with caution. Considering the error bar indicating +/– 1 standard deviation in Fig. 1b, positive SAM during strong La Niña years is most robust feature. This is mainly because mean value of SAM indices for strong La Niña years is far from zero than that for El Niño years. Interestingly, in moderate La Niña cases, the mean value is negative, which is opposite response with the strong La Niña case. Although it is difficult to interpret robustly because the error bar is too wide, this seems to indicate the nonlinearity in the SAM response for La Niña cases.

Correlation analysis using the all 57 (54) years indicates that

Table 3. Same as Table 2 except for using +/– 1°C as a threshold level which divides total ENSO events into the strong and moderate ENSO categories.

	Case	Niño 3.4 (1957-2013)	CTI (1957-2010)
1	Total	**–0.29 (57)**	**–0.27 (54)**
2	Strong ENSO	**–0.58* (21)**	**–0.52 (21)**
3	Moderate ENSO	+0.4 (16)	+0.34 (15)

the Niño 3.4 (CTI) index is negatively correlated with the SAM index; this correlation is statistically significant at the 95% confidence level (Table 2). However, this correlation is sensitive to the definition of the austral summer season and length of time analyzed. With the shorter period (1979-2010), the correlation is not statistically significant at 95% confidence level (not shown). LT obtained a statistically significant negative correlation between the two indices for the interval from November to February, even with a shorter period of analysis (1979-2010). Wang and Cai (2013) estimated correlation between the SAM and ENSO indices for 1870-2010, which is a much longer period than that used for this study; they obtained robust negative correlations before 1920s and after 1960s, but between those two periods, they identified a weak positive relation instead, although this correlation was not robust or statistically significant.

As anticipated, for the years in the strong ENSO category, we obtained a strong negative correlation between ENSO and

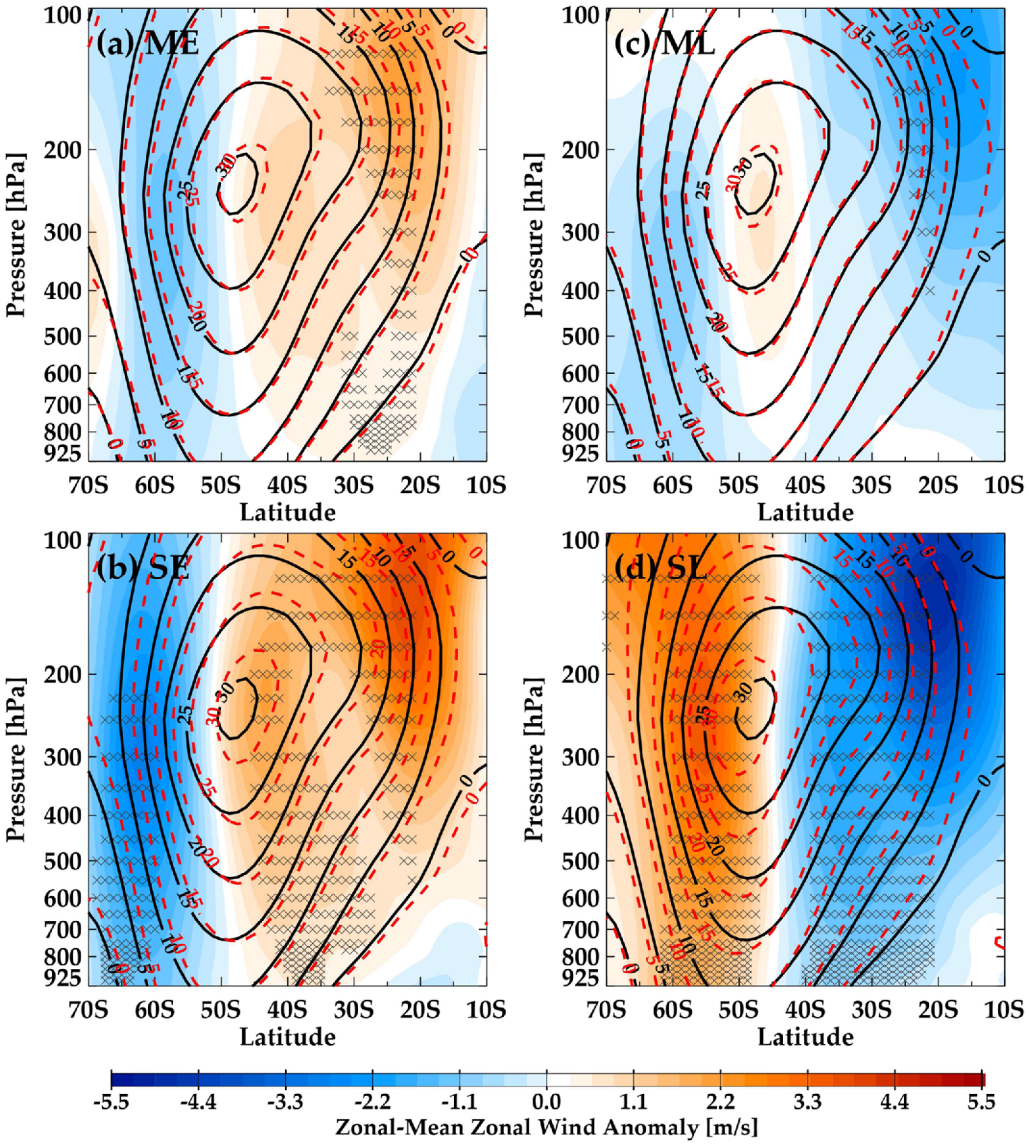

Fig. 3. JRA-55 zonal-mean zonal wind (red dashed contours) and anomalies (shading) from climatology (black solid contours) with different ENSO strengths, (a) ME, (b) SE, (c) ML, and (d) SL. The negative and positive zonal-mean zonal wind anomalies are shaded in blue and red respectively. Crosses indicate regions significant at the 95% confidence level.

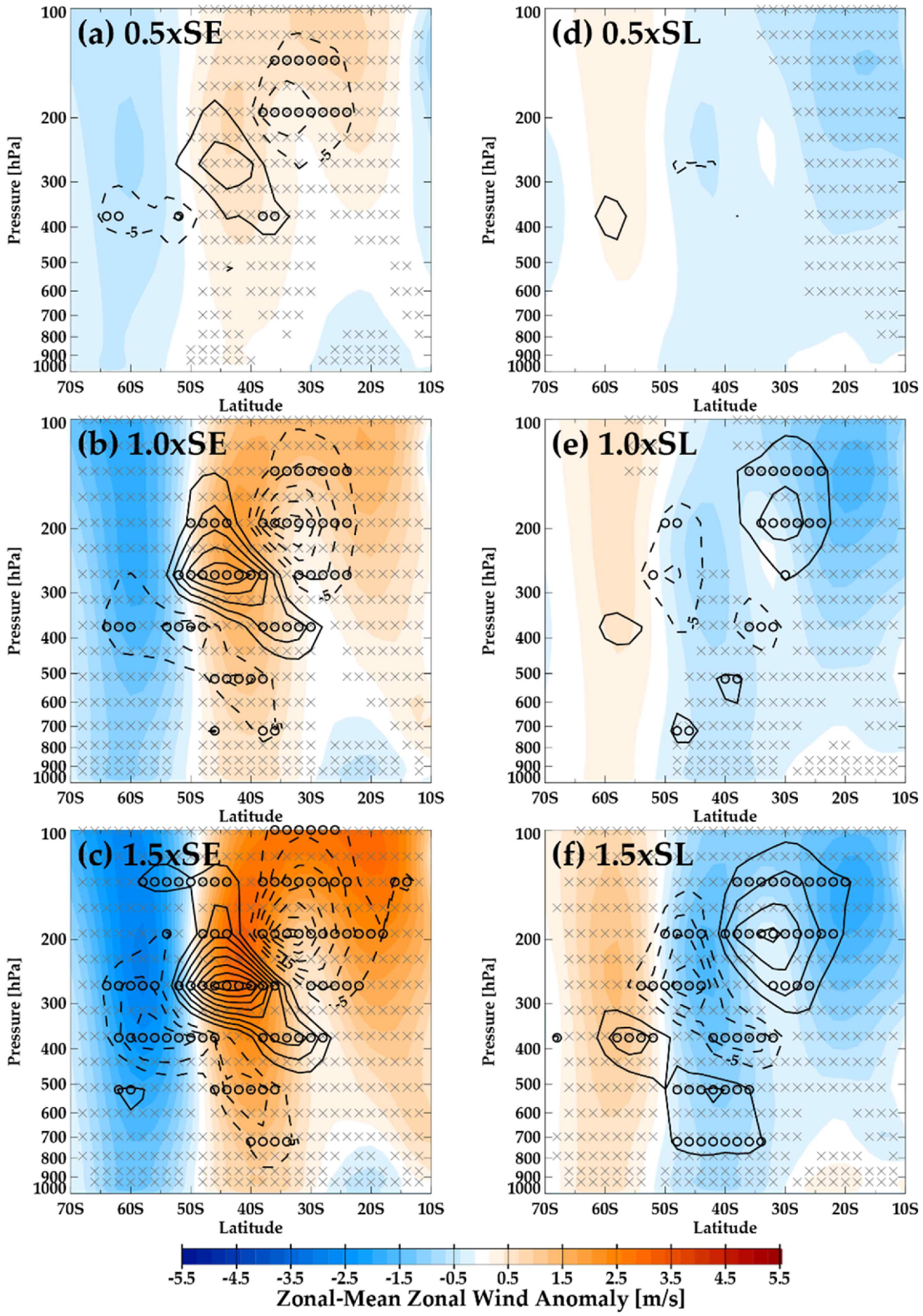

Fig. 4. Modeled EP flux divergence/convergence anomalies (solid/dashed contours) in 3-8 day eddies with different amplification factors: (a, d) $\alpha = 0.5$, (b, e) $\alpha = 1.0$, and (c, f) $\alpha = 1.5$ for cases of (left column) El Niño and (right column) La Niña. Color-shaded regions show modeled zonal-mean zonal wind anomalies. The contour interval is 5 kg m^{-1} s^{-2}, and the zero line is omitted. Crosses (open circles) indicate regions that the zonal-mean zonal wind anomalies (EP flux divergence/convergence anomalies) are significant at the 95% confidence level.

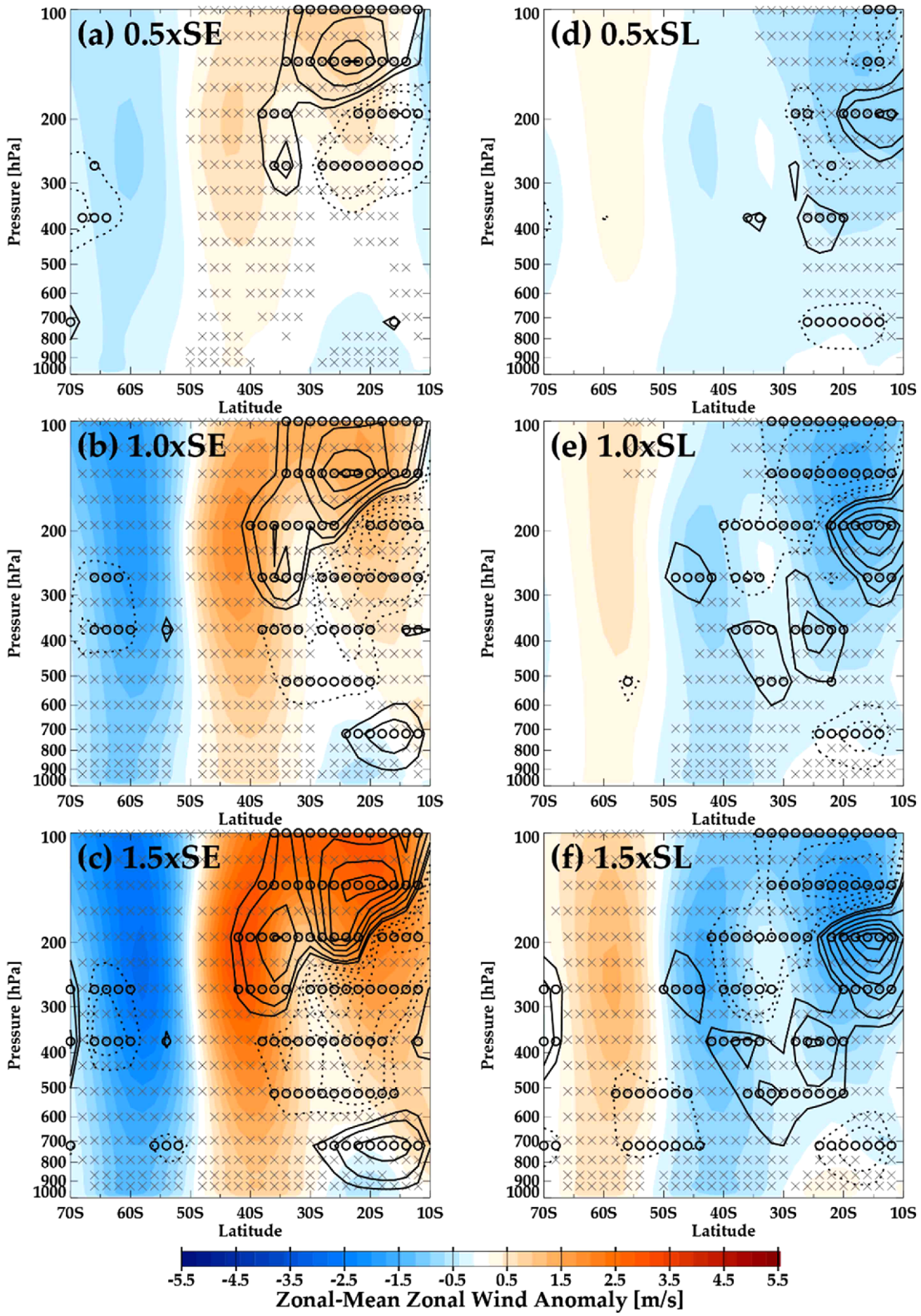

Fig. 5. Modeled EP flux divergence/convergence (solid/dashed contours) anomalies of DJF stationary waves [kg m^{-1} s^{-2}], cases of (left column) El Niño, (right column) La Niña. The contour interval is double from Fig. 4, and ± 5 [kg m^{-1} s^{-2}] contours are added for visualization. Crosses (open circles) indicate regions that the zonal-mean zonal wind anomalies (EP flux divergence/convergence anomalies) are significant at the 95% confidence level.

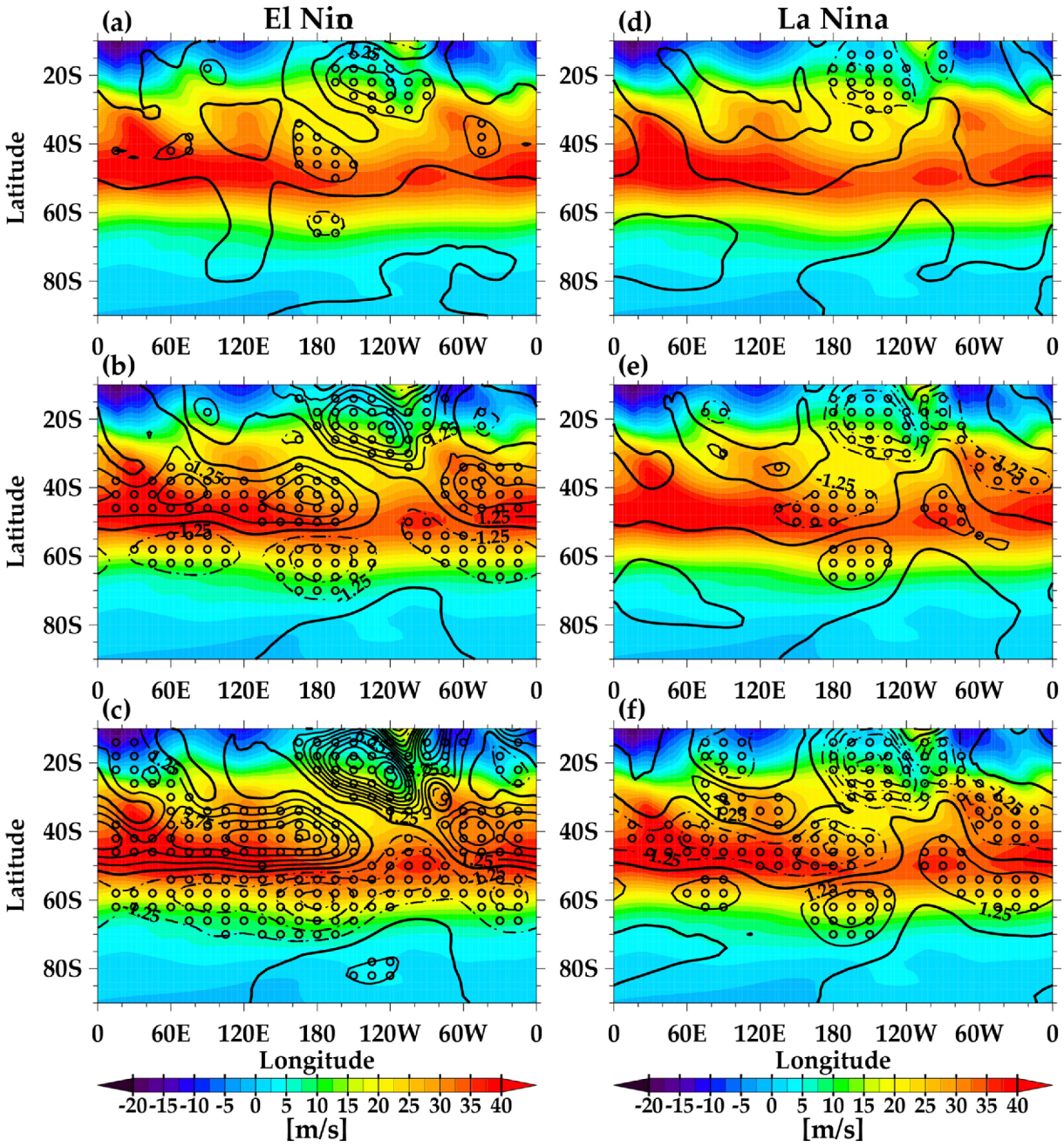

Fig. 6. Modeled zonal wind climatology (shading) and anomalies from the climatology (contours) at 200 hPa: cases of (left column) El Niño and (right column) La Niña. From top to bottom, these figures show the modeled results with the amplification factors of 0.5, 1.0, and 1.5. The contour interval is 1.25 m s^{-1}, and the shading interval is 2.5 m s^{-1}. The solid and dashed lines indicate positive and negative values, respectively. The open circles indicate the significant regions at 95% confidence level.

the SAM that was significant at the 99% confidence level (Table 2); On the other hand, the correlation was insignificant and even opposite, i.e. a positive correlation between ENSO and SAM, for the years in the moderate ENSO category. These results are insensitive to the specific choice of ENSO index. Therefore, the relationship between ENSO and the SAM depends on the ENSO amplitude, and the relationship between the two indices is not as strong as was suggested in previous studies (LT; Gong et al., 2010). We further check the sensitivity of the correlation analysis results (Table 2) on the threshold level (+/– 1.5°C) by changing it to +/– 1°C (Table 3).

Composite analysis was conducted on zonal-mean zonal wind data to examine how the latitudinal and vertical structure of the SPJ changes according to the different strengths of the ENSO event, based on the years representing each ENSO category (Fig. 3). Changes in zonal-mean zonal wind ano-

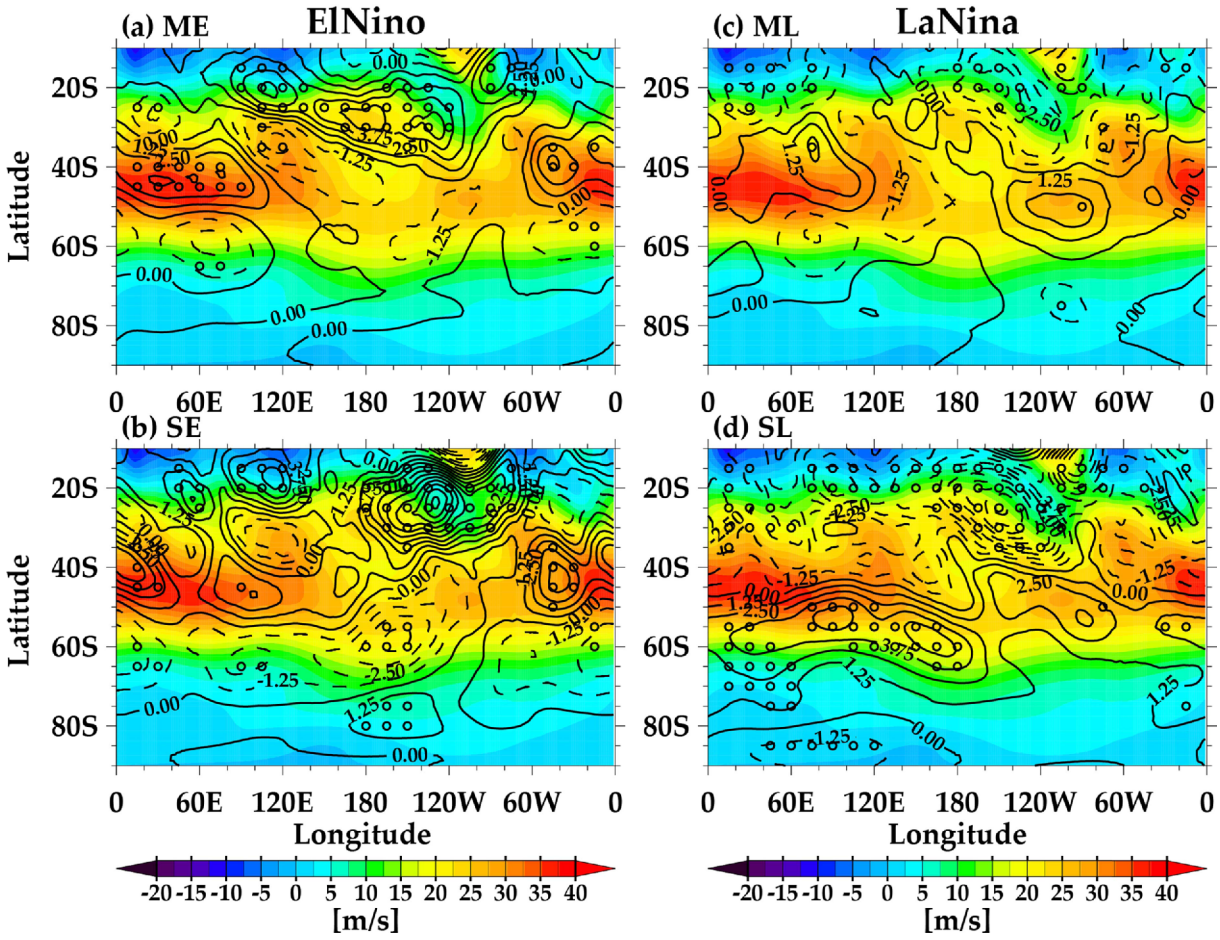

Fig. 7. JRA-55 zonal wind climatology (shading) and anomalies from the climatology (contour) at 200 hPa: cases of (left column) El Niño and (right column) La Niña. Contour interval is 1.25 m s^{-1}, and shading interval is 2.5 m s^{-1}. Thick solid and dashed lines indicate positive and negative values, respectively. The open circles indicate the significant regions at 95% confidence level.

malies of the SPJ were significant for the strong El Niño (La Niña) category, and the anomalies were associated with the northward (southward) displacement of the SPJ (red dashed line, Figs. 3b and 3d). For both cases, the vertical structures of the zonal-mean zonal wind anomalies were similar and nearly equivalent barotropic with peaks at 300 hPa. However, the latitudinal band that exhibits significant wind modification differs. For the case of a strong El Niño, deceleration was significant in the 55°S-65°S latitude band, whereas acceleration mainly occurred at 50°S-60°S in the case of a strong La Niña, which is consistent with the findings of previous studies (e.g., Limpasuvan and Hartmann, 1999; Turner et al., 2009). In the case of a moderate El Niño (La Niña), no significant modification to the strength or position of zonal-mean zonal wind is observed (Figs. 3a and 3c). It is worthwhile to indicate the contrasting characteristics of moderate El Niño and La Niña cases in the zonal mean responses. For the moderate La Niña case in particular, easterly wind anomalies occur over the southern high-latitude area, which is a notably different pattern from that of a strong La Niña. Unlike with the El Niño cases, which show linear responses with respect to the increasing magnitudes of El Niño forcing, the responses for the La Niña between strong and moderate cases are completely different particularly in the extratropics implying that the nonlinear response of SAM might be contributed by the La Niña cases to a large extent. However, caution is needed in this interpretation because features in moderate cases are not significant at all.

b. Modeling results

In previous section, we showed that a robust statistical relationship exists between SAM and ENSO in the strong ENSO cases. Although the relationship is quite robust (99% significance level), the statistical test is conducted only with 12 members (6 for El Niño and 6 for La Niña cases). To further confirm the amplitude-dependent relationship between SAM and ENSO, the relationship is examined with a suite of general circulation model experiments. Figure 4 shows the model responses of zonal-mean zonal wind anomalies from the climatology (color shaded). For all experiments, the anomalous zonal-mean zonal winds have equivalent barotropic structure with opposite signs centered at around 40°S and 60°S, re-

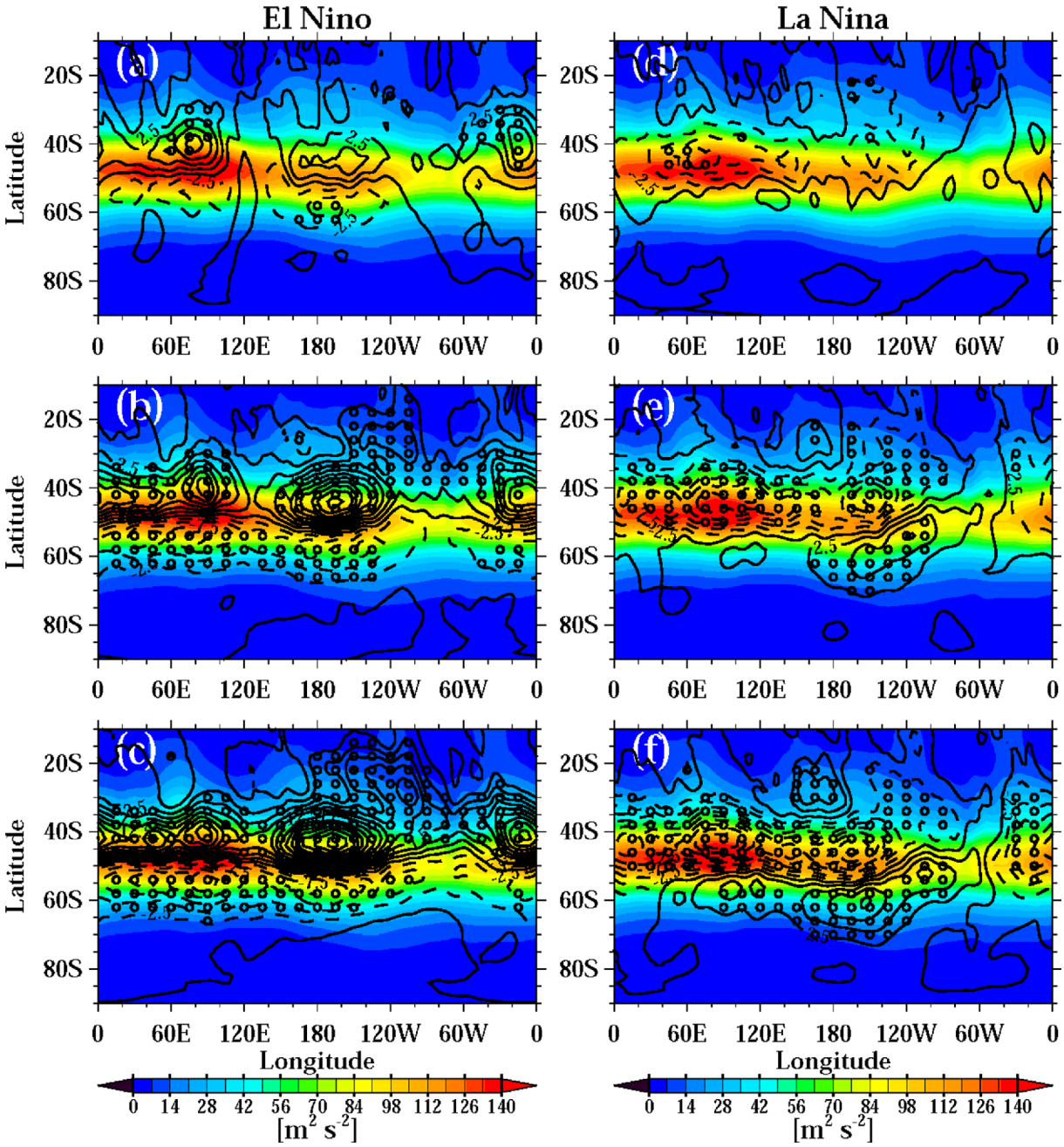

Fig. 8. Modeled storm track climatology (shading) and anomalies from the climatology (contours) at 200 hPa for the cases of (left column) El Niño and (right column) La Niña. From top to bottom, panels show the simulation results for amplification factors of 0.5, 1.0, and 1.5. Contour interval is 2.5 $m^2 s^{-2}$ from −40 $m^2 s^{-2}$, and shading interval is 7 $m^2 s^{-2}$ from 0 $m^2 s^{-2}$. The solid and dashed lines indicate positive and negative values, respectively. The storm track is represented by the $\overline{v'^2}$, where v is meridional wind, overbar is time mean, and prime is deviation from the time mean, respectively. The open circles indicate the significant regions at 95% confidence level.

spectively (color shaded). Notably, for smallest amplification factors (Figs. 4a and 4d), the zonal-mean zonal wind response is insignificant, which is consistent with the observational composite analysis result depicted in Fig. 3. In case of model response with amplification factor 1 (Figs. 4b and 4e), which corresponds to the strong case in Fig. 3, there exists an asymmetry in the model response between El Niño and La Niña case. In El Niño case (Fig. 4b), a clear reduction of zonal-mean zonal wind anomalies is simulated well in the latitudinal band between 50°S and 70°S and this is consistent result with the observational composite analysis (Fig. 3). However, still, non-significant response is obtained in the La Niña case (Fig. 4e). Note that this feature is contrasting with the composite analysis (Fig. 3d). Especially, the southern extratropical zonal

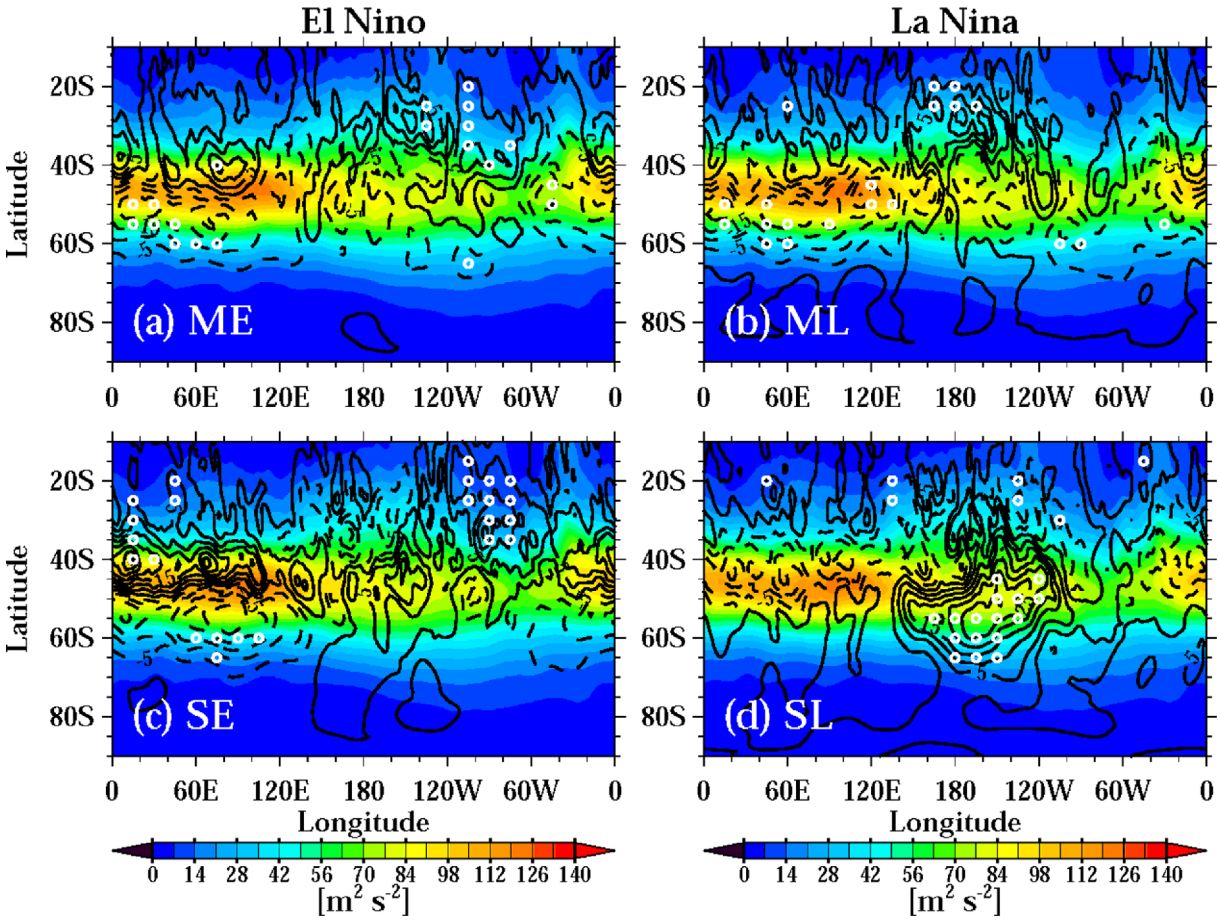

Fig. 9. JRA-55 storm track climatology (shading) and anomalies from the climatology (contours) at 200 hPa for the cases of (left column) El Niño and (right column) La Niña. From top to bottom, panels show the composite results for moderate and strong cases. Contour interval is 5 $m^2 s^{-2}$ from −40 $m^2 s^{-2}$, and shading interval is 7 $m^2 s^{-2}$ from 0 $m^2 s^{-2}$. The solid and dashed lines indicate positive and negative values, respectively. The storm track is represented by the $\overline{v'^2}$, where v is meridional wind, overbar is time mean, and prime is deviation from the time mean, respectively. The open circles indicate the significant regions at 95% confidence level.

wind response is much weaker than it is during El Niño. When amplification factor reaches to 1.5, both El Niño and La Niña cases show opposite responses in the southern extratropical zonal-mean zonal wind anomalies, eventually. However, note that amplification 1.5 is rather exaggerating value in simulating the ENSO variability.

Figure 4 also shows the changes in the EP flux divergence of transient eddies, which is a measure of transient eddy forcing, in response to the gradual increase of ENSO SST forcing (contour). In general, near 60°S, where the upper-level zonal-mean wind response is strongest, the EP flux convergence (divergence) decelerated (accelerated) zonal-mean wind in case of El Niño (La Niña) and this is consistent with southern extratropical zonal mean wind response (shaded). Note that, in La Niña case with $\alpha = 1$, EP flux divergence (Fig. 4e) near 60°S is no bigger than that with $\alpha = 0.5$. Therefore, in La Niña case simulated by the model, transient eddy forcing becomes significant and modulates southern extratropical zonal mean wind when La Niña becomes unrealistically bigger than observed one.

The role of stationary eddy in the zonal-mean zonal wind change was also examined (Fig. 5). EP flux convergence induced by the stationary eddies was relatively small compared to those from transient eddies and also was less sensitive to increase in ENSO SST forcing. Notably, in cases of La Niña, the eddy forcings shown in Figs. 4d-f were found to be much weaker than those of the El Niño cases. Therefore, the non-significant response in La Nina case with amplification factor 1 (Fig. 3d) can be ascribed to the relatively weaker tropical forcings that are applied during La Niña case (Fig. 2).

Since the model response is strongest at upper-level, we further investigate the modeled responses of zonal wind anomalies at 200 hPa under the different strengths (Fig. 6). As expected, upper-level zonal wind responses are amplified as El Niño forcing becomes bigger (Figs. 6a-c). The salient feature revealed by the model simulation is the existence of zonally elongated wind anomalies with a north/south dipolar structure centered at 40°S, 60°S, and 180°E. Because the dipolar anomaly straddles the climatological jet at 50°S (shading), this

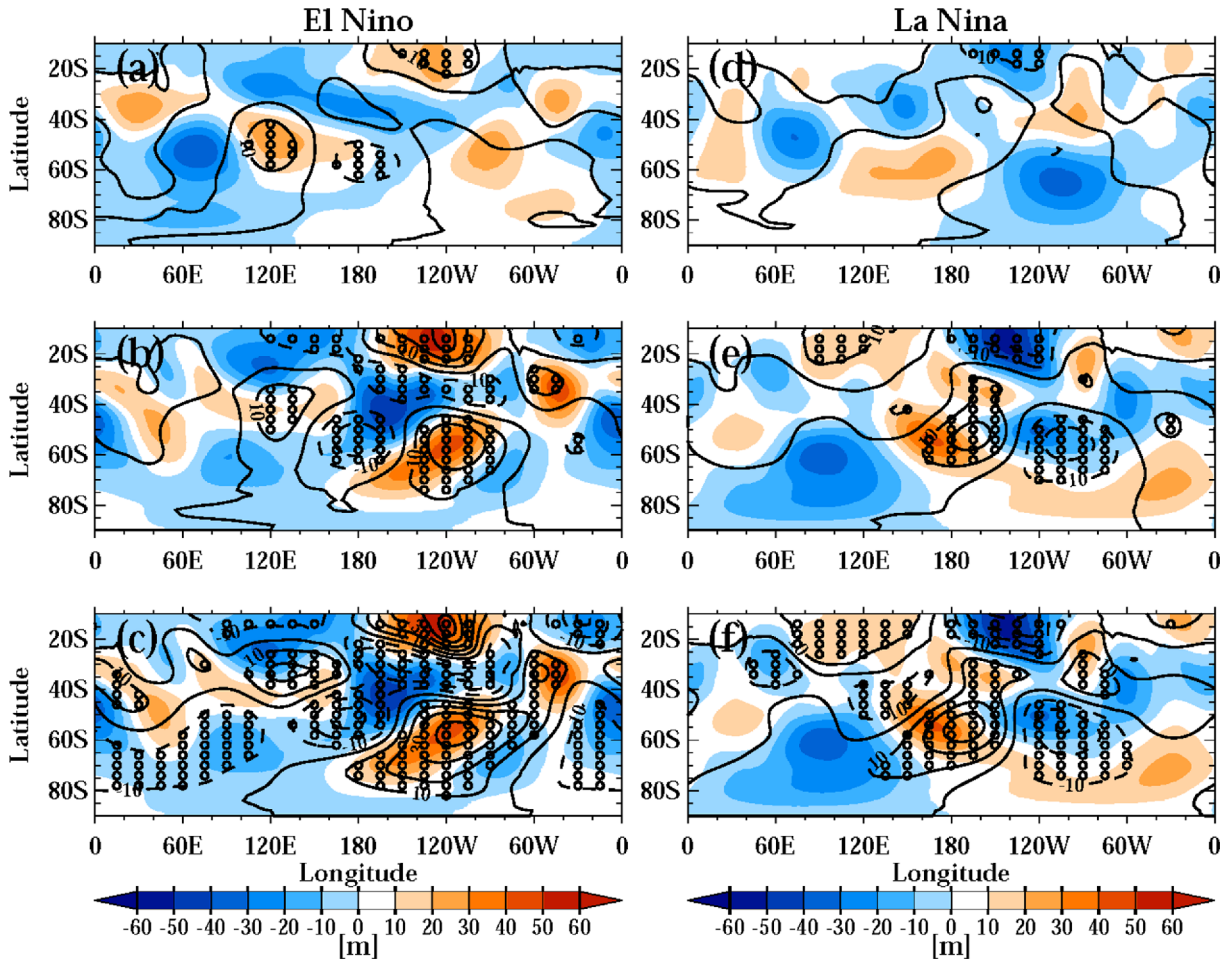

Fig. 10. Modeled (contours) and JRA-55 (shading) DJF stationary eddies. The level is 200 hPa for both models. Zonal-mean removed geopotential height anomalies from climatology are used: cases of (left column) El Niño and (right column) La Niña. The numbers in parentheses refer to the amplification factors. The first row ($\alpha = 0.5$) is compared with the JRA-55 moderate ENSO results, and the second and third rows ($\alpha = 1.0$ and 1.5) are compared with the JRA-55 strong ENSO results. Contour and shading intervals are 10 m. The solid and dashed lines indicate positive and negative values, respectively. The open circles indicate the significant regions at 95% confidence level.

structure indicates the equatorward shift of the SPJ in response to strong El Niño. It should be noted that with amplification factors of 0.5 and 1.0 (Figs. 6a-b), the magnitudes of the induced dipolar anomalies are less than 5% of the maximum wind speed of the climatological SPJ, which indicates that this response is relatively small.

In the case of La Niña forcing, major zonal wind anomalies were similar, but opposite in sign from the El Niño cases. Because the zonal wind dipole occurs at similar location, but with the opposite sign, the resulting impacts on the climatological SPJ are also opposite, i.e., poleward shift of the SPJ. This result is consistent with those of previous studies. However, in contrast to the case of El Niño, the modeled response with an amplification factor of 1.5 with La Niña (Fig. 6f) has a marginally larger amplitude relative to the other cases (Figs. 6d-e). In addition, the magnitude is smaller than to that of the corresponding El Niño case (Fig. 6c).

For comparison with observational analysis, we provide upper-level zonal wind composite features for both moderate and strong ENSO cases in Fig. 7. Comparison of the composite upper-level zonal wind data with the corresponding model results (Fig. 6) reveals that, in particular, the model responses capture the observed composite features well in strong ENSO cases. However, the model responses cannot reproduce detailed features of moderate ENSO cases for both El Niño and La Niña.

In light of the robust shift of the SPJ revealed in the modeled zonal wind responses (Fig. 6), we examined how transient eddies respond to ENSO forcing (Fig. 8). For this study, transient eddies were identified with 3-8-day filtered fields (Duchon, 1979). Notably, meridional wind variance ($\overline{v'^2}$) at 200 hPa was shifted equatorward (poleward) for cases of El Niño (La Niña). This model simulation result is very similar with the meridional wind variance at 200 hPa obtained from

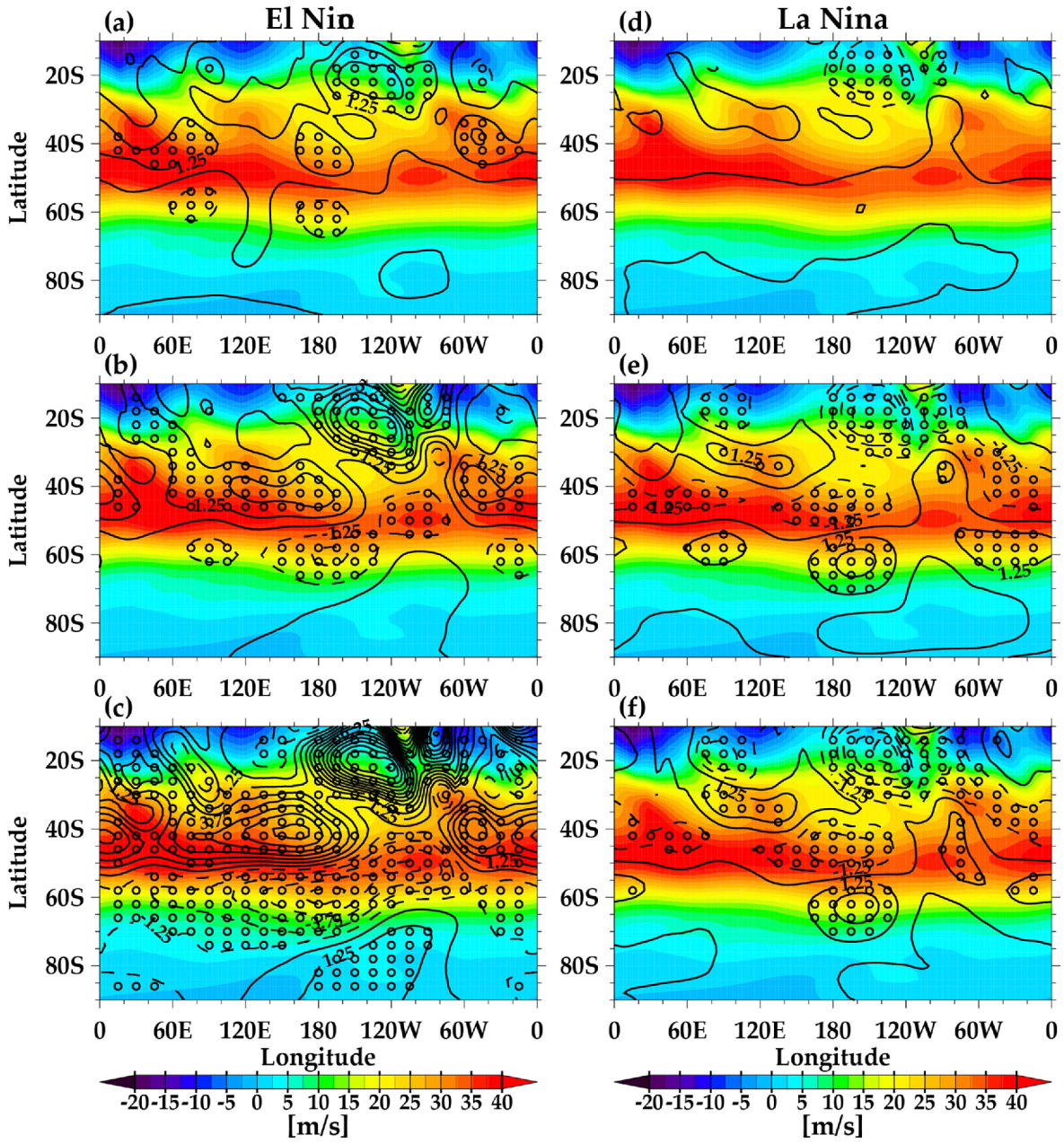

Fig. 11. Same as Fig. 6 except for simulation results of T-ENSO experiments.

observational composite analysis (Fig. 9). Comparing Figs. 6 and 8, a clear correspondence is apparent between the upper-level zonal wind and meridional wind variance, which indicates that the modeled transient baroclinic eddies indeed respond to increases and decreases in the upper-level zonal wind response. These results are consistent with previous studies that emphasized the changes in vertical wind shear during ENSO (e.g., Robinson, 2000; Lorenz and Hartmann, 2001; Chen and Plumb, 2009; Zurita-Gotor et al., 2014). Model-simulated stationary eddies at upper level responding to ENSO forcing of different strengths (Fig. 10, contours) capture the observed stationary eddies (shading) reasonably well. During the El Niño conditions in particular, a characteristic bow-like wave propagation pattern emanates from the tropical western Pacific in both the model and the observed composite analysis; this pattern is similar to the recently identified teleconnection pattern associated with western Antarctic warming (e.g., Ding et al., 2011). Note that the stationary wave response tends to be larger with stronger El Niño SST anomalies. However, the contribution to the southern extratropical zonal mean wind induced by the stationary eddy forcing is relatively smaller than the transient eddy forcing contribution and is less sensitive to the increased ENSO SST forcing (Fig. 5). In cases of La Niña, both the modeled and observed

composite stationary eddies were weaker than those in the El Niño cases. Consequently, the eddy forcings shown in Figs. 5d-f were also found to be much weaker than those of the El Niño cases.

ENSO-related teleconnection is known to induce distinct SST anomalies in the Southern Ocean by enhancing turbulent heat flux and Ekman heat transport (e.g., Li, 2000; Renwick, 2002; Verdy et al., 2006; Ciasto and Thompson, 2008; Ciasto and England, 2011; Simpkins et al., 2012). Surface cyclogenesis over the open ocean is most likely to occur in regions with the strongest meridional SST gradient, called oceanic frontal zones (Sinclair, 1994). Since the boundary conditions applied to our modelling experiments already contain the ENSO-induced extratropical SST anomalies, it is worthwhile to examine how much eddy forcing is contributed by the extratropical SST forcing indirectly driven by tropical ENSO signal. To address this issue, we devised another set of experiments in which only subtropical SST distributions were used; these are referred to as 'T-ENSO experiments'. For these T-ENSO experiments, we superimposed SST anomalies with six different amplitudes confined to the region of 24.5°S-24.5°N. For the remaining regions, the anomalies were set to zero. We chose this specific band of latitude to minimize discontinuities between the forced and the unforced subtropical regions as much as possible. Other conditions are identical with those described in section 2. As a result, SST changes in the extratropical region during the ENSO were found to be minor in the ENSO teleconnection, at least in the southern hemisphere, because the model simulation results were qualitatively similar with both global and tropically confined ENSO forcings.

Figure 11 shows the upper-level zonal wind responses of the T-ENSO experiments. Because of the large differences in the SST gradients over the mid-latitude southern Pacific Ocean during El Niño and La Niña periods (Fig. 2), we expected that reduction of baroclinicity along the intensified oceanic fronts seem to reduce the magnitude of eddy forcings. However, rather surprisingly, the results of the T-ENSO experiments are almost similar with those with original experiments (Fig. 6), which indicates that the zonal wind in southern extratropics is intrinsically induced by tropical ENSO forcing, and that the extratropical response is caused by subsequent atmospheric dynamical adjustment processes in the extratropics. In this case, we can infer that the southern extratropical SST patterns that occur during ENSO events are subsequent oceanic responses to the induced extratropical atmospheric forcing. Additional impacts from the induced extratropical SST can be regarded as minor.

4. Summary and discussion

Through observational analysis and a series of modeling experiments, we investigated the origin of the amplitude-dependent relationship between the SAM and ENSO indices in the austral summer. From the observational analysis, we found that the relationship is only robust when ENSO forcing is sufficiently strong. Although the majority of ENSO cases are moderate, data reconstructed without strong ENSO cases did not show significant correlation with SAM for the analyzed period. In this study, we addressed this issue in detail using GCM simulations. Based on the composite analysis using reanalysis data and the GCM experiments, the relative roles of stationary and transient eddy forcings induced by ENSO with different amplitudes were examined by calculating the EP flux and its divergence or convergence. Major findings from both the analysis and the modeling experiments are that transient eddy forcing is significantly amplified in strong ENSO, and therefore this forcing plays a major role in driving the amplitude-dependent relationship between the SAM and ENSO. Moderate tropical SST forcing was not sufficient to drive these eddy-induced changes in westerly flow. However, note that this result does not imply that the way ENSO influences the SAM is distinctly different in the weaker ENSO cases. In cases of La Niña, zonal wind response is much weaker than it is during El Niño, and both transient and stationary wave forcings were relatively weak compared to those during El Niño. Partly, this difference is ascribed to the relatively weak tropical forcings that are applied during La Niña. These modelling results support that El Niño SST condition is more effective in the production of both stationary and transient eddy forcings in the southern extratropical region compared to the La Niña SST condition. Although further studies are needed, this suggests a possibility that the nonlinear response of La Niña cases as depicted in Fig. 3 might be ascribed to the less efficient eddy forcing during La Niña case.

Previous study revealed that the correlation between SAM and ENSO is not uniform but exhibits multi-decadal fluctuations (Wang and Cai, 2013). Since our study suggests that the existence of significant correlation is mainly due to the strong ENSO events, it is possible that the correlation between strong ENSO and SAM in the weak correlation period would actually be stronger if the correlation analysis discards events other than the strong ones. Therefore, it is also possible that the multi-decadal fluctuations of the correlation could be related with the fluctuations in the number of strong ENSO events with decade.

As a final remark, we address one of inconsistent features of the model simulations compared with the observational analysis. It is the weaker model response of SAM during the strong La Niña. Note that the SAM response is stronger in the observed composite analysis for strong La Niña rather than strong El Niño case (Fig. 3). Although this feature does not change the major conclusion described above, further study is needed to understand the observed nonlinear behavior of SAM during the La Niña cases.

Acknowledgements. This work was supported by the project "Investigation of Climate Change Mechanism by Observation and Simulation of Polar Climate for the Past and Present" (PE16010) of the Korea Polar Research Institute.

Edited by: Soon-Il An

References

Andrews, D. G., J. R. Holton, and C. B. Leovy, 1987: *Middle Atmosphere Dynamics*. Academic Press, 489 pp.

Barnes, E., D. L. Hartmann, D. M. W. Frierson, and J. Kidston, 2010: Effect of latitude on the persistence of eddy-driven jet. *Geophys. Res. Lett.*, **37**, L11804, doi:10.1029/2010GL043199.

Chen, G., and P. Zurita-Gotor, 2008: The tropospheric jet response to prescribed zonal forcing in an idealized atmospheric model. *J. Atmos. Sci.*, **65**, 2254-2271, doi:10.1175/2007JAS2589.1.

_____, and R. A. Plumb, 2009: Quantifying the eddy feedback and the persistence of the zonal index in an idealized atmospheric model. *J. Atmos. Sci.*, **66**, 3707-3720, doi:10.1175/ 2009JAS3165.1.

Ciasto, L. M., and D. W. J. Thompson, 2008: Observations of large-scale ocean-atmosphere interaction in the Southern Hemisphere. *J. Climate*, **21**, 1244-1259, doi:10.1175/2007JCLI1809.1.

_____, and M. H. England, 2011: Observed ENSO teleconnections to Southern Ocean SST anomalies diagnosed from a surface mixed layer heat budget. *Geophys. Res. Lett.*, **38**, L09701, doi:10.1029/2011-GL046895.

Compo, G. P., and P. D. Sardeshmukh, 2004: Storm track predictability on seasonal and decadal scales. *J. Climate*, **17**, 3701-3720, doi:10.1175/1520-0442(2004)017<3701:STPOSA>2.0.CO;2.

Ding, Q., E. J. Steig, D. S. Battisti, and M. Kuttel, 2011: Winter warming in West Antarctica caused by central tropical Pacific warming. *Nat. Geosci.*, **4**, 398-403, doi:10.1038/ngeo1129.

_____, _____, _____, and J. M. Wallace, 2012: Influence of the tropics on the Southern Annular Mode. *J. Climate*, **25**, 6330-6348, doi:10.1175/JCLI-D-11-00523.1.

Duchon, C. E., 1979: Lanczos filtering in one and two dimensions. *J. Appl. Meteorol.*, **18**, 1016-1022, doi:10.1175/1520-0450(1979)018<1016:LFIOAT>2.0.CO;2.

Edmon, H. J., B. J. Hoskins, and M. E. McIntyre, 1980: Eliassen-Palm cross sections for the troposphere. *J. Atmos. Sci.*, **37**, 2600-2616, doi:10.1175/1520-0469(1980)037<2600:EPCSFT>2.0.CO;2.

Eichler, T., and W. Higgins, 2006: Climatology and ENSO-related variability of North American extratropical cyclone activity. *J. Climate*, **19**, 2076-2093, doi:10.1175/JCLI3725.1.

Gong, D. Y., and S. W. Wang, 1998: Antarctic oscillation: concept and applications. *Chin. Sci. Bull.*, **43**, 734-738, doi:10.1007/BF02898949.

Gong, T., S. B. Feldstein, and D. Luo, 2010: The impact of ENSO on wave breaking and Southern Annular Mode events. *J. Atmos. Sci.*, **67**, 2854-2870, doi:10.1175/2010JAS3311.1.

_____, _____, and _____, 2013: A simple GCM study on the Relationship between ENSO and the Southern Annular Mode. *J. Atmos. Sci.*, **70**, 1821-1832, doi:10.1175/JAS-D-12-0161.1.

Harangozo, S. A., 2000: A search for ENSO teleconnections in the west Antarctic Peninsula climate in Austral winter. *Int. J. Climatol.*, **20**, 663-679, doi:10.1002/(SICI)1097-0088(200005)20:6<663::AID-JOC493>3.0.CO;2-I.

Harnik, N., R. Seager, N. Naik, M. Cane, and M. Ting, 2010: The role of linear wave refraction in the transient eddy-mean flow response to tropical Pacific SST anomalies. *Quart. J. Roy. Meteor. Soc.*, **136**, 2132-2146, doi:10.1002/qj.688.

Hartmann, D. L., 2007: The atmospheric general circulation and its variability. *J. Meteor. Soc. Japan,* **85**, 123-143, doi:10.2151/jmsj.85B.123.

Hoerling, M. P., and M. Ting, 1994: Organization of extratropical transients during El Niño. *J. Climate*, **7**, 745-766, doi:10.1175/1520-0442(1994)007<0745:OOETDE>2.0.CO;2.

Hoskins, B. J., and D. J. Karoly, 1981: The steady linear response of a spherical atmosphere to thermal and orographic forcing. *J. Atmos. Sci.*, **38**, 1179-1196, doi:10.1175/1520-0469(1981)038<1179:TSLROA>2.0.CO;2.

Karoly, D. J., 1989: Southern Hemisphere circulation features associated with El Nino-Southern Oscillation events. *J. Climate*, **2**. 1239-1252, doi:10.1175/1520-0442(1989)002<1239:SHCFAW>2.0.CO;2.

Kidson, J. W., 1988: Interannual variations in the Southern Hemisphere circulation. *J. Climate*, **1**, 1177-1198, doi:10.1175/1520-0442(1988)001<1177:IVITSH>2.0.CO;2.

Kobayashi, S., and Coauthors, 2015: The JRA-55 reanalysis: General specifications and basic characteristics. *J. Meteor. Soc. Japan,* **93**, 5-48, doi:10.2151/jmsj.2015-001.

Kug, J. S., F. F. Jin, and S. I. An, 2009: An Two types of El Niño events: Cold tongue El Niño and warm pool El Niño. *J. Climate*, **22**, 1499-1515, doi:10.1175/2008JCLI2624.1.

Kushnir, Y., W. A. Robinson, I. Bladé, N. M. J. Hall, S. Peng, and R. Sutton, 2002: Atmospheric GCM response to extratropical SST anomalies: Synthesis and evaluation. *J. Climate*, **15**, 2233-2256, doi:10.1175/1520-0442(2002)015,2233: AGRTES.2.0.CO;2.

Kwok, R., and J. C. Comiso, 2002: Spatial patterns of variability in Antarctic surface temperature: Connections to the Southern Hemisphere Annular Mode and the Southern Oscillation. *Geophys. Res. Lett.*, **29**, 1705, doi:10.1029/2002GL015415.

L'Heureux, M. L., and D. W. J. Thompson, 2006: Observed relationships between the El Niño-Southern Oscillation and the extratropical zonal-mean Circulation. *J. Climate*, **19**, 276-287, doi:10.1175/JCLI3617.1.

Li, Z., 2000: Influence of tropical Pacific El Niño on the SST of the Southern Ocean through atmospheric bridge. *Geophys. Res. Lett.*, **27**, 3505-3508, doi:10.1029/1999GL011182.

Lim, E. P., H. Hendon, and H. Rashid, 2013: Seasonal predictability of the Southern Annular Mode due to its association with ENSO. *J. Climate*, **26**, 8037-8054, doi:10.1175/JCLI-D-13-00006.1.

Limpasuvan, V., and D. L. Hartmann, 1999: Eddies and the annular modes of climate variability. *Geophys. Res. Lett.*, **26**, 3133-3136, doi:10.1029/1999GL010478.

Lorenz, D. J., and D. L. Hartmann, 2001: Eddy-zonal flow feedback in the Southern Hemisphere. *J. Atmos. Sci.*, **58**, 3312-3327, doi:10.1175/1520-0469(2001)058,3312: EZFFIT.2.0.CO;2.

Lu, J., G. Chen, and D. M. W. Frierson, 2008: Response of the zonal mean atmospheric circulation to El Nino versus global warming. *J. Climate*, **21**, 5835-5851, doi:10.1175/2008JCLI2200.1.

Lu, J., L. Sun, Y. Wu, and G., Chen, 2014: The role of subtropical irreversible PV mixing in the zonal mean circulation response to global warming-like thermal forcing. *J. Climate*, **27**, 2297-2316, doi:10.1175/JCLI-D-13-00372.1.

Marshall, G. J., 2003: Trends in the Southern Annular Mode from observations and reanalyses. *J. Climate*, **16**, 4134-4143, doi:10.1175/1520-0442(2003)016<4134:TITSAM>2.0.CO;2.

Nie, Y., Y. Zhang, G. Chen, X. Q. Yang, and D. A. Burrows, 2014: Quantifying barotropic and baroclinic eddy feedbacks in the persistence of the Southern Annular Mode. *Geophys. Res. Lett.*, **41**, 8636-8644, doi:10.1002/2014GL062210.

Orlanski, I., 2005: A new look at the Pacific storm track variability: Sensitivity to tropical SSTs and to upstream seeding. *J. Atmos. Sci.*, **62**, 1367-1390, doi:10.1175/JAS3428.1.

Rayner, N. A., D. E. Parker, E. B. Horton, C. K. Folland, L. V. Alexander, D. P. Rodwell, E. C. Kent, and A. Kaplan, 2003: Global analyses of sea surface temperature, sea ice, and night marine air temperature since the late nineteenth century. *J. Geophys. Res.*, **108**, 4407, doi:10.1029/2002-JD002670.

Renwick, J. A., 2002: Southern Hemisphere circulation and relations with sea ice and sea surface temperature. *J. Climate*, **15**, 3058-3068, doi:10.1175/1520-0442(2002)015<3058:SHCARW>2.0.CO;2.

Rivière, G., 2009: Effect of latitudinal variations in low-level baroclinicity on eddy life cycles and upper-tropospheric wave- breaking processes. *J. Atmos. Sci.*, **66**, 1569-1592, doi:10.1175/ 2008JAS2919.1

Robinson, W. A., 2000: A baroclinic mechanism for the eddy feedback on the zonal index. *J. Atmos. Sci.*, **57**, 415-422, doi:10.1175/1520-0469 (2000)057,0415:ABMFTE.2.0.CO;2.

Robinson, W. A., 2002: On the midlatitude thermal response to tropical warmth. *Geophys. Res. Lett.*, **29**, 1190, doi:10.1029/2001GL014158.

Schubert, S. D., M. J. Suarez, P. J. Pegion, R. D. Koster, and J. T. Bacmeister, 2004a: Causes of long-term drought in the U.S. Great Plains. *J. Climate*, **17**, 485-503, doi:10.1175/1520-0442(2004)017 <0485:COLDIT>2.0.CO;2.

_____, _____, _____, _____, and _____, 2004b: On the cause of the 1930s dust bowl. *Science*, **303**, 1855-1859, doi:10.1126/science.1095048.

Seager, R., 2007: The turn of the century North American drought: Global context, dynamics, and past analogs. *J. Climate*, **20**, 5527-5552, doi:10.1175/2007JCLI1529.1.

Seager, R., Y. Kushnir, C. Herweijer, N. Naik, and J. Velez, 2005: Modeling of tropical forcing of persistent droughts and pluvials over western North America: 1856-2000. *J. Climate*, **18**, 4068-4091, doi: 10.1175/JCLI3522.1.

Seager, R., Y. Kushnir, M. Ting, M. Cane, N. Naik, and J. Miller, 2008: Would advance knowledge of 1930s SSTs have allowed prediction of the dust bowl drought? *J. Climate*, **21**, 3261-3281, doi:10.1175/ 2007JCLI2134.1.

Simpkins, G. R., L. M. Ciasto, D. W. J. Thompson, and M. H. England, 2012: Seasonal relationships between large-scale climate variability and Antarctic sea ice concentration. *J. Climate*, **25**, 5451-5469, doi:10.1175/ JCLI-D-11-00367.1.

Sinclair, M. R., 1994: An objective cyclone climatology for the Southern Hemisphere. *Mon. Wea. Rev.*, **122**, 2239-2256, doi:10.1175/1520-0493 (1994)122<2239:AOCCFT>2.0.CO;2.

Smith, T. M., R. W. Reynolds, T. C. Peterson, and J. Lawrimore, 2008: Improvements to NOAA's historical merged land-ocean surface temperature analysis (1880-2006). *J. Climate*, **21**, 2283-2296, doi:10. 1175/2007JCLI2100.1.

Straus, D. M., and J. Shukla, 1997: Variations of midlatitude transient dynamics associated with ENSO. *J. Atmos. Sci.*, **54**, 777-790, doi:10. 1175/1520-0469(1997)054<0777:VOMTDA>2.0.CO;2.

Thompson, D. W. J., and J. M. Wallace, 2000: Annular Modes in the extra-tropical circulation. Part I: Month-to-Month Variability*. *J. Climate*, **13**, 1000-1016, doi:10.1175/1520-0442(2000)013<1000:AMITEC>2.0.CO;2.

Trenberth, K. E., and J. W. Hurrell, 1994: Decadal atmosphere-ocean variations in the Pacific. *Climate Dyn.*, **9**, 303-319, doi:10.1007/ BF00204745.

Turner, J., R. A. Bindschadler, P. Convey, G. Prisco, E. Fahrbach, J. Gutt, D. Hodgson, P. A. Mayewski, and C. Summerhayes, 2009: *Antarctic Climate Change and the Environment*. Scientific Committee on Antarctic Research, 526 pp.

Verdy, A., J. Marshall, and A. Czaja, 2006: Sea surface temperature variability along the path of the Antarctic Circumpolar Current. *J. Phys. Oceanogr.*, **36**, 1317-1331, doi:10.1175/JPO2913.1.

Wang, G., and W. Cai, 2013: Climate-change impact on the 20th-century relationship between the Southern Annular Mode and global mean temperature. *Sci. Rep.*, **3**, 2039, doi:10.1038/srep02039.

Wang, Y. H., and G. Magnusdottir, 2011: Tropospheric Rossby wave breaking and the SAM. *J. Climate*, **24**, 2134-2146, doi:10.1175/ 2010JCLI4009.1.

Yu, J. Y., H. Paek, E. S. Saltzman, and T. Lee, 2015: The early 1990s change in ENSO-PSA-SAM relationships and its impact on Southern Hemisphere climate. *J. Climate*, **28**, 9393-9408, doi:10.1175/JCLI-D-15-0335.1.

Zurita-Gotor, P., J. Blanco-Fuentes, and E. P. Gerber, 2014: The impact of baroclinic eddy feedback on the persistence of jet variability in the two-layer model. *J. Atmos. Sci.*, **71**, 410-429, doi:10.1175/JAS-D-13-0102.1.